Title: GNS561, a clinical-stage PPT1 inhibitor, has powerful antitumor activity against hepatocellular carcinoma via modulation of lysosomal functions

Sonia Brun[1, #, *, 15], Eric Raymond[1, 2, #], Firas Bassissi[1], Zuzana Macek Jilkova[3, 4, 5], Soraya Mezouar[1], Madani Rachid[1], Marie Novello[1], Jennifer Tracz[1], Ahmed Hamaï[6, 7], Gilles Lalmanach[8, 9], Lise Vanderlynden[8, 9], Eloïne Bestion[1, 10], Raphael Legouffe[11], Jonathan Stauber[12], Thomas Schubert[13], Maximilian G. Plach[13], Jérôme Courcambeck[1], Cyrille Drouot[1], Guillaume Jacquemot[1], Cindy Serdjebi[1], Gael Roth[3, 4, 5], Jean-Pierre Baudoin[14], Christelle Ansaldi[1], Thomas Decaens[3, 4, 5,#] and Philippe Halfon[1, #, *]

[1]Genoscience Pharma, Marseille, France

[2]Medical Oncology, Paris Saint-Joseph Hospital, Paris, France

[3]Institute for Advanced Biosciences, Research Center UGA / Inserm U 1209 / CNRS 5309, La Tronche, France

[4]University Grenoble Alpes, Faculté de médecine, France

[5]Clinique Universitaire d'Hépato-gastroentérologie, Pôle Digidune, CHU Grenoble, France

[6]Institut Necker-Enfants Malades, Inserm U1151-CNRS UMR 8253, Paris, France

[7]University Paris Descartes-Sorbonne Paris Cité, Paris, France

[8]INSERM, UMR1100, Centre d'Etude des Pathologies Respiratoires, Equipe "Mécanismes Protéolytiques dans l'Inflammation", Tours, France

[9]Tours University, Tours, France

[10]CNRS, IRD, MEPHI, IHU Méditerranée Infection, Aix Marseille University, Marseille, France

[11]ImaBiotech, Loos, France

[12]ImaBiotech, Billerica, USA

[13]2Bind GmbH, Regensburg, Germany

[14]Aix Marseille University, IRD, APHM, MEPHI, IHU Méditerranée Infection, Marseille, France

[15]Lead contact

[#] These authors contributed equally

*Correspondence: brun.sonia@hotmail.fr and p.halfon@genosciencepharma.com

SUMMARY

Hepatocellular carcinoma (HCC) is the most frequent primary liver cancer. Autophagy inhibitors have been extensively studied in cancer but, to date, none has reached efficacy in clinical trials. In this study, we demonstrated that GNS561, a new autophagy inhibitor, whose anticancer activity was previously linked to lysosomal cell death, displayed high liver tropism and potent antitumor activity against a panel of human cancer cell lines and in two HCC in vivo models. We showed that GNS561, which is an effective lysosomotropic agent, can reach and inhibit its enzyme target, palmitoyl-protein thioesterase 1, resulting in lysosomal unbound Zn^{2+} accumulation, impairment of cathepsin activity, blockage of autophagic flux, altered location of mTOR, lysosomal membrane permeabilization, caspase activation and cell death. Accordingly, GNS561, currently tested in a global Phase 1b/2a clinical trial against primary liver cancer, represents a promising new drug candidate and a hopeful therapeutic strategy in cancer treatment.

Keywords: GNS561, liver cancer, lysosome, PPT1, autophagy, lysosomotropism, antitumor, zinc, mTOR

INTRODUCTION

With an estimated 782,000 deaths in 2018, hepatocellular carcinoma (HCC) stands as the most common primary liver cancer and constitutes the fourth leading cause of cancer-related death worldwide (Bray et al. 2018). The rising incidence of HCC, the high worldwide mortality rate, and limited therapeutic options at advanced stages, make HCC a significant unmet medical need.

Autophagy-related lysosomal cell death, either alone or in connection with several other cell death pathways, has been recognized as a major target for cancer therapy (Aits and Jaattela 2013). Dysregulated autophagic-lysosomal activity and mTOR signaling were shown to allow cancer cells to become resistant to the cellular stress induced by chemotherapy and targeted therapy (Klempner et al. 2013). Recently, several lysosome-specific inhibitors were shown to target palmitoyl-protein thioesterase 1 (PPT1), resulting in the modulation of protein palmitoylation and antitumor activity in melanoma and colon cancer models (Rebecca et al. 2017, Rebecca et al. 2019). PPT1 palmitoylates proteins, enabling their degradation and intracellular trafficking of membrane-bound proteins. This process was shown to play a central role in the control of cellular autophagy. PPT1 was reported to be highly expressed in several cancer cell lines as well as in advanced stage cancers in patients (Rebecca et al. 2019).

Chloroquine (CQ) and hydroxychloroquine (HCQ) have been used for more than 50 years to prevent and treat malarial infections and autoimmune diseases. Based on the lysosomotropic properties and the capacity for autophagy inhibition, these molecules have been proposed as active drugs in cancer (Dolgin 2019, Pérez-Hernández et al. 2019) and have been extensively investigated in recent years (Kimura et al. 2013, Manic et al. 2014, Zhang et al. 2015, Shi et al. 2017, Verbaanderd et al. 2017, Xu et al. 2018). Over 40 clinical trials have been reported to evaluate the activity of both CQ or HCQ as single agent or in combination with chemotherapy in several tumor types (Manic et al. 2014, Shi et al. 2017, Verbaanderd et al. 2017). However, the required drug concentrations to inhibit autophagy were not achieved in humans, leading to inconsistent results in cancer clinical trials (Pascolo 2016, Rebecca et al. 2017, Plantone and Koudriavtseva 2018). This prompted research to identify novel compounds with potent inhibitory properties against autophagy for cancer therapy.

80 We previously reported that GNS561 was efficient in intrahepatic cholangiocarcinoma (iCCA)
81 by inhibiting late-stage autophagy and inducing a dose-dependent build-up of enlarged
82 lysosomes (Brun et al. 2019). In this study, we investigated the lysosomotropism of GNS561
83 and then the disruption of related lysosomal functions such as autophagy and lysosomal
84 enzymatic activity. We also identified lysosomal PPT1 as a target GNS561. Exposure to
85 GNS561 was shown to induce lysosomal unbound zinc ion (Zn^{2+}) accumulation, inhibition of
86 PPT1 and cathepsin activity, blockage of autophagic flux and mTOR displacement.
87 Interestingly, these effects resulted in lysosomal membrane permeabilization (LMP) and
88 caspase activation that led to cancer cell death. This mechanism was associated with dose-
89 dependent inhibition of cancer cell proliferation and tumor growth inhibition in several HCC
90 in vivo models. These data establish PPT1 and lysosomes as major targets for cancer cells
91 and led to the development of a clinical program investigating the effects of GNS561 in
92 patients with advanced HCC.
93
94

RESULTS

GNS561 displays activity against human cancer cell lines and patient-derived cells

The effects of GNS561 on cell viability were investigated in a panel of human cancer cell lines, including HCC, iCCA and colon, renal cell, breast, prostate, lung, and ovarian carcinoma as well as acute myeloid leukemia, glioblastoma, and melanoma. As shown in Table 1, GNS561 showed potent antitumor activity ranging from 0.22 ± 0.06 µM for the most sensitive cell line (LN-18, a glioblastoma cell line) to 7.27 ± 1.71 µM for the least sensitive cell line (NIH:OVCAR3, an ovarian cancer cell line). GNS561 was at least 10-fold more effective than HCQ in cultured cancer cells. GNS561 also displayed activity in primary HCC patient-derived cells and was on average 3-fold more potent than sorafenib, a reference drug in HCC treatment (mean IC_{50} 3.37 ± 2.40 µM for GNS561 vs 10.43 ± 4.09 µM for sorafenib).

		Mean IC_{50} ± SD (µM)	
Cancer type	Cell lines	GNS561	HCQ
Colon Carcinoma	HCT-116	1.22 ± 0.15	14.41 ± 1.5
	HT-29	1.35 ± 0.04	24.18 ± 5.14
Renal Cell Carcinoma	786-O	1.72 ± 0.17	21.65 ± 3.15
	CAKI-1	1.10 ± 0.19	17.69 ± 1.29
Ovarian Cancer	NIH:OVCAR3	7.27 ± 1.71	98.01 ± 12.75
Melanoma	A375	1.2 ± 0.13	12.27 ± 2.8
	SK-MEL-28	1.81 ± 0.5	22.78 ± 2.65
Breast Cancer	MDA-MB-231	2.17 ± 0.14	14.13 ± 3.06
Prostate Cancer	DU-145	1.09 ± 0.18	45.74 ± 0.55
	PC-3	2.56 ± 0.23	43.43 ± 6.04
Lung Cancer	A549	1.69 ± 0.34	14.33 ± 1.59
	NCI-H358	2.54 ± 0.34	54.07 ± 14.19
HCC	HepG2	0.47 ± 0.15	11.55 ± 1.52
	Huh7	0.88 ± 0.31	13.62 ± 0.71
Glioblastoma	LN-229	0.60 ± 0.24	10.87 ± 1.23
	LN-18	0.22 ± 0.06	5.27 ± 0.74
Acute Myeloid Leukemia	KG-1	5.86 ± 1.64	43.92 ± 2.76
	Mean	1.99 ± 1.86	27.52 ± 23.28

	IC_{50} (µM)	
Primary HCC patient-derived cells	GNS561	sorafenib
LI0050	3.54	9.12
LI0574	2.41	8.65
LI0612	6.93	17.94
LI0752	0.49	6.34
LI0801	2.07	5.7
LI1005	3.16	14.49
LI1098	6.95	10.85
LI1646	1.44	10.33
Mean	3.37 ± 2.40	10.43 ± 4.09

106 **Table 1.** In vitro activity of GNS561 and HCQ in human cancer cell lines (left, IC_{50} ± SD, µM)
107 and in vitro activity of GNS561 and sorafenib in primary hepatocellular carcinoma (HCC)
108 patient-derived cells (right, IC_{50}, µM).
109
110 **GNS561 has antitumor properties in HCC in vivo models**
111 The whole-body tissue distribution of GNS561 was investigated in rats after repeated oral
112 administration of GNS561 at a dose of 40 mg/kg/day for 28 days. Seven hours after the last
113 administration, the GNS561 level was measured by mass spectrometry imaging in the liver,
114 lung, stomach, brain, eye, salivary gland, kidney, heart, fat, muscle, testis, and skin (Figure 1).
115 GNS561 mainly accumulated in the liver, stomach and lung as shown by the calculated
116 organ/blood ratio (Figure 1B). Lower concentrations of GNS561 were also detected in eyes,
117 skin, brain and testis, indicating that GNS561 crosses the blood/brain barrier and the
118 blood/testis barrier to a limited extent (brain to blood and testis to blood ratios were 0.21
119 and 0.40, respectively).
120

121

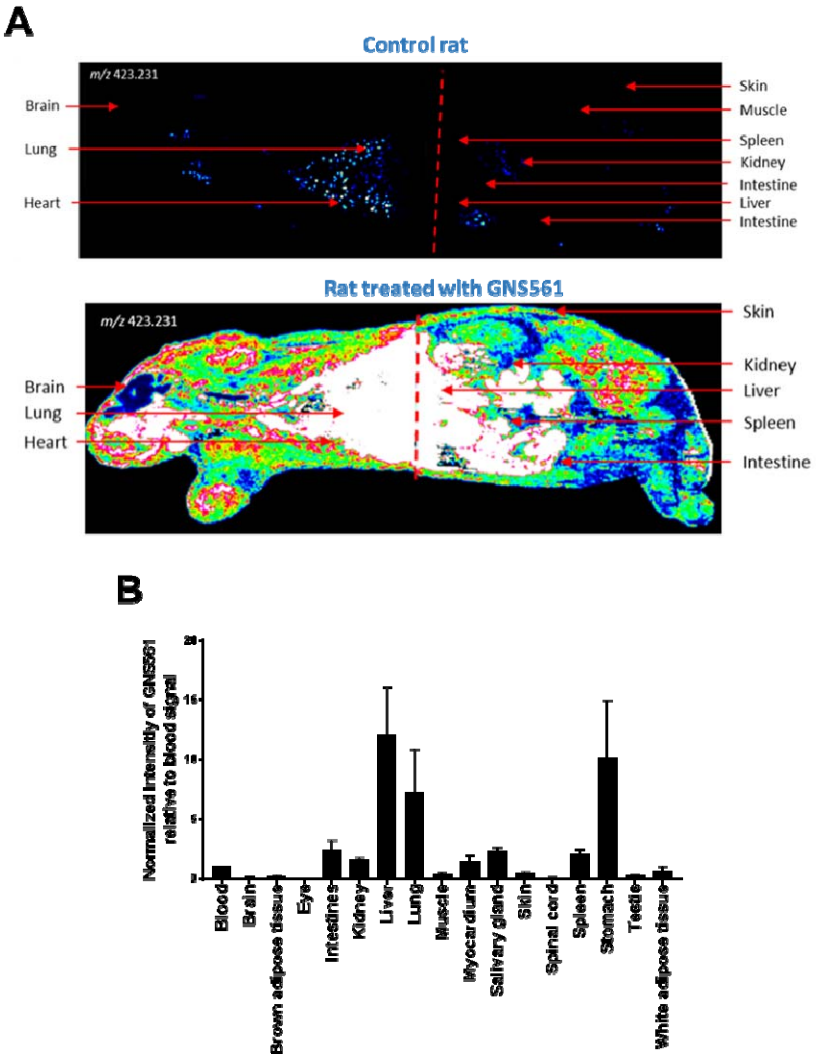

122

123 **Figure 1. Whole body tissue distribution of GNS561.** (A) Mass spectrometry imaging of a
124 control rat (top) and a rat treated with GNS561 at a dose of 40 mg/kg/day for 28 days
125 (bottom). (B) Normalized intensity of GNS561 relative to blood signal in several organs of
126 GNS561-treated rats (Mean + SEM, n=2 except for eye, n=1). Of note, the GNS561 liver-to-
127 blood ratio is underestimated due to liver signal saturation.

128

129 Based on the high concentrations of GNS561 in the liver and potent in vitro activity against
130 HCC cells, the effects of GNS561 were investigated in vivo using two liver cancer models,
131 including the human HCC orthotopic patient-derived LI0752 xenograft mouse model and the
132 diethylnitrosanime (DEN)-induced immunocompetent rat HCC model.
133 In the HCC patient-derived LI0752 xenograft BALB/c nude mouse model, tumor volume and
134 weight were reduced by 37.1% and 34.4%, respectively, in mice treated with GNS561 at 50

135 mg/kg compared to the control (Figure S1A and B). Consistently, GNS561 treatment induced
136 a decrease in serum AFP levels in a dose-dependent manner and was significantly different
137 from the control at days 21 and 28 after treatment (Figure S1C-G).
138 Since HCC often develops in cirrhotic livers in humans, we further characterized the
139 antitumor effects of GNS561 in a DEN-induced cirrhotic rat model of HCC. Rats with already
140 developed HCC were either treated with sorafenib at 10 mg/kg, GNS561 at 15 mg/kg, or the
141 combination of both drugs (Figure S2). In this model, tumor progression was significantly
142 reduced by sorafenib (33.0%) and GNS561 (33.0%) compared to an untreated control group,
143 and the greatest decrease in tumor progression was observed by the combination (68%) that
144 displayed an additive effect (Figure 2A). Magnetic resonance imaging analyses further
145 showed a significant increase in the mean tumor size of 9.97 ± 0.97 mm in control rats
146 compared to 6.45 ± 0.35 mm with sorafenib, 5.48 ± 1.00 mm in GNS561 and 3.83 ± 0.52 mm
147 in the combination group (Figure 2B). Following liver resection, the macroscopic counting of
148 tumor nodules revealed significantly lower numbers in all treated groups compared to the
149 control group (Figure 2C). Immunohistochemical analyses of liver tumors showed a
150 significantly lower Cyclin D1-positive nuclear staining in the tumors of rats treated with
151 GNS561 or by the combination of GNS561 with sorafenib compared to the control group
152 (Figure 2D). GNS561 and combination treatments also significantly reduced Ki67 staining
153 compared to the control group (Figure 2E). The effects on Cyclin D1 and Ki67 were primarily
154 related to GNS561 exposure, as sorafenib alone showed no statistically significant
155 differences in Cyclin D1 or Ki67 staining compared to the control group. Our results further
156 showed that GNS561 and the combination treatment did not interfere with lipid or glucose
157 metabolism or kidney function but slightly affected some liver functions (Table S1).
158

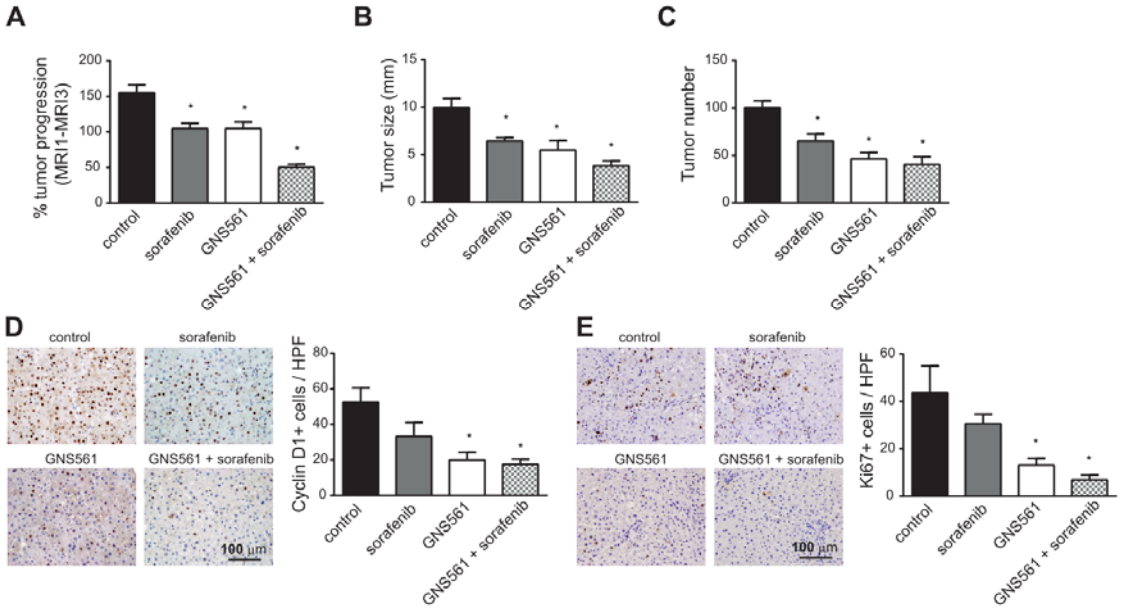

Figure 2. GNS561 activity in a diethylnitrosanime-induced cirrhotic rat model of hepatocellular carcinoma. (A) Tumor progression assessment by comparison of tumor size obtained by magnetic resonance imaging (MRI) 1 and MRI 3 in the control, sorafenib at 10 mg/kg, GNS561 at 15 mg/kg and combination (GNS561 + sorafenib) groups. Macroscopic examination of livers with assessments of (B) tumor size and (C) tumor number at the surface of livers. (D) Representative images of nuclear Cyclin D1 staining and quantification of Cyclin D1-positive staining per high-power field (HPF). (E) Representative images of nuclear Ki67-positive staining and quantification of Ki67 staining per HPF. For all studies, mice n ≥ 6 per group. Data represent the mean + SEM. Comparison of means was performed by one-way ANOVA with Dunnett's post hoc analysis. * represents significant difference, at least $p < 0.05$.

GNS561 activates the caspase-dependent apoptosis pathway

We further wanted to characterize the antitumor effect of GNS561 and to determine whether GNS561 could trigger apoptotic cell death. To this end, annexin V/propidium iodide (PI) analysis was performed by flow cytometry after 48 h of GNS561 exposure in HepG2 cells. Early (Annexin V+/PI- staining) and late (Annexin V+/PI+ staining) apoptosis increased in a dose-dependent manner after GNS561 exposure (Figure 3A). The induction of apoptosis was confirmed by immunodetection of poly-ADP-ribose polymerase cleavage in GNS561-treated cells (Figure 3B). We further examined whether GNS561-induced apoptosis was related to

180 caspase activation. After 6 h of exposure, GNS561 had no effect on caspase 8 and caspase
181 3/7 activity in HepG2 cells (Figure 3C). In contrast, activation of caspase 8 and caspase 3/7
182 was observed after 24 h of treatment with GNS561, and this effect was sustained at 30 h. A
183 decrease in cell viability was concomitant with caspase activation (Figure 3C). The induction
184 of caspase activation was confirmed by flow cytometry (Figure 3D) and by detection of
185 cleavage of caspase 3 using immunoblot analysis (Figure 3E). Moreover, to confirm that
186 GNS561-induced cell death is caspase-dependent apoptosis, pretreatment (1 h) with the
187 cell-permeable pan-caspase inhibitor Z-VAD-FMK (5 µM) was performed. Cell viability was
188 restored in the presence of Z-VAD-FMK (Figure 3F), further confirming that GNS561 induced
189 a caspase-dependent apoptotic cell death.

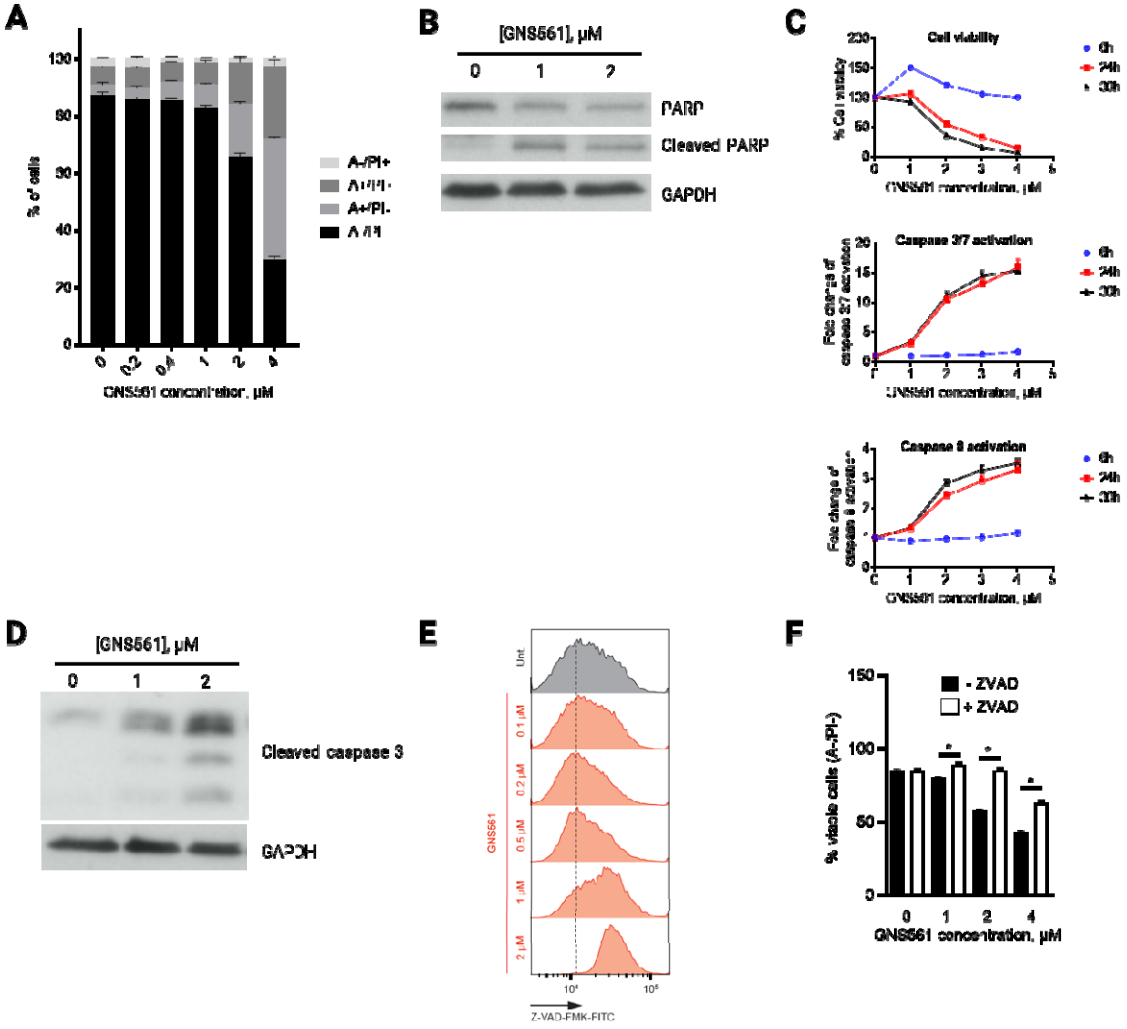

190

191 **Figure 3. GNS561 induces apoptotic cell death in HepG2 cells in a dose and time-dependent**
192 **manner through caspase activatio**n. (A) Annexin V (A)/propidium iodide (PI) analysis by flow

193 cytometry after 48 h of GNS561 treatment. (B) Representative immunoblotting of the
194 cleaved and non-cleaved forms of poly-ADP-ribose polymer (PARP) after 24 h of GNS561
195 treatment. (C) Cell viability and activation of caspase 3/7 and 8 after 6, 24 and 30 h of
196 treatment with GNS561. (D) Representative immunoblotting of cleaved caspase 3 levels
197 after 24 h of treatment with GNS561. (E) Caspase-glow analysis by flow cytometry after 48 h
198 of treatment with GNS561. (F) Viable cell (A-/PI-) analysis by flow cytometry after
199 pretreatment with Z-VAD-FMK (ZVAD) at 5 µM for 1 h and then treatment with ZVAD at 5
200 µM and GNS561 for 48 h. For all blots, GAPDH was used as a loading control. For all studies,
201 n ≥ 3 biological replicates. Data represent the mean + SEM. For comparison, Student t-test
202 was used. * represents significant difference, at least $p < 0.05$.
203
204 **GNS561 is a lysosomotropic agent**
205 The intracellular localization of GNS561 in HepG2 cells was visualized using GNS561D, the
206 photoactivable analog of GNS561 containing a diazide moiety (Figure 4A). GNS561D showed
207 a punctuate fluorescent signal that colocalized with the intracellular vesicle-like structure
208 stained by LAMP1 (Figure 4B), demonstrating that GN561 accumulated in lysosomes and is a
209 lysosomotropic agent. Pretreatment with NH_4Cl, a weak base that rapidly increases
210 lysosomal pH, was further used to validate the lysosomotropic character of GNS561. As
211 shown in Figure 4B, NH_4Cl pretreatment strongly prevented lysosomal accumulation of
212 GNS561D. Then, we investigated whether GNS561 lysosomotropism was related to induced
213 cell death. For this purpose, HepG2 cells were pretreated for 2 h with NH_4Cl and then
214 treated with GNS561 for 24 h. Although a concentration of 20 mM NH_4Cl alone slightly
215 decreased viability (Figure 4C), it significantly attenuated the larger decrease in viability
216 induced by GNS561. These results were confirmed by pretreatment with bafilomycin A1 (Baf
217 A1), an inhibitor of the vacuolar H+-ATPase (Figure S3). Therefore, disrupting GNS561
218 lysosomal localization protected against GNS561-mediated cell death. These results
219 suggested that GNS561 antitumor activity in HepG2 cells is caused by its lysosomotropism.
220

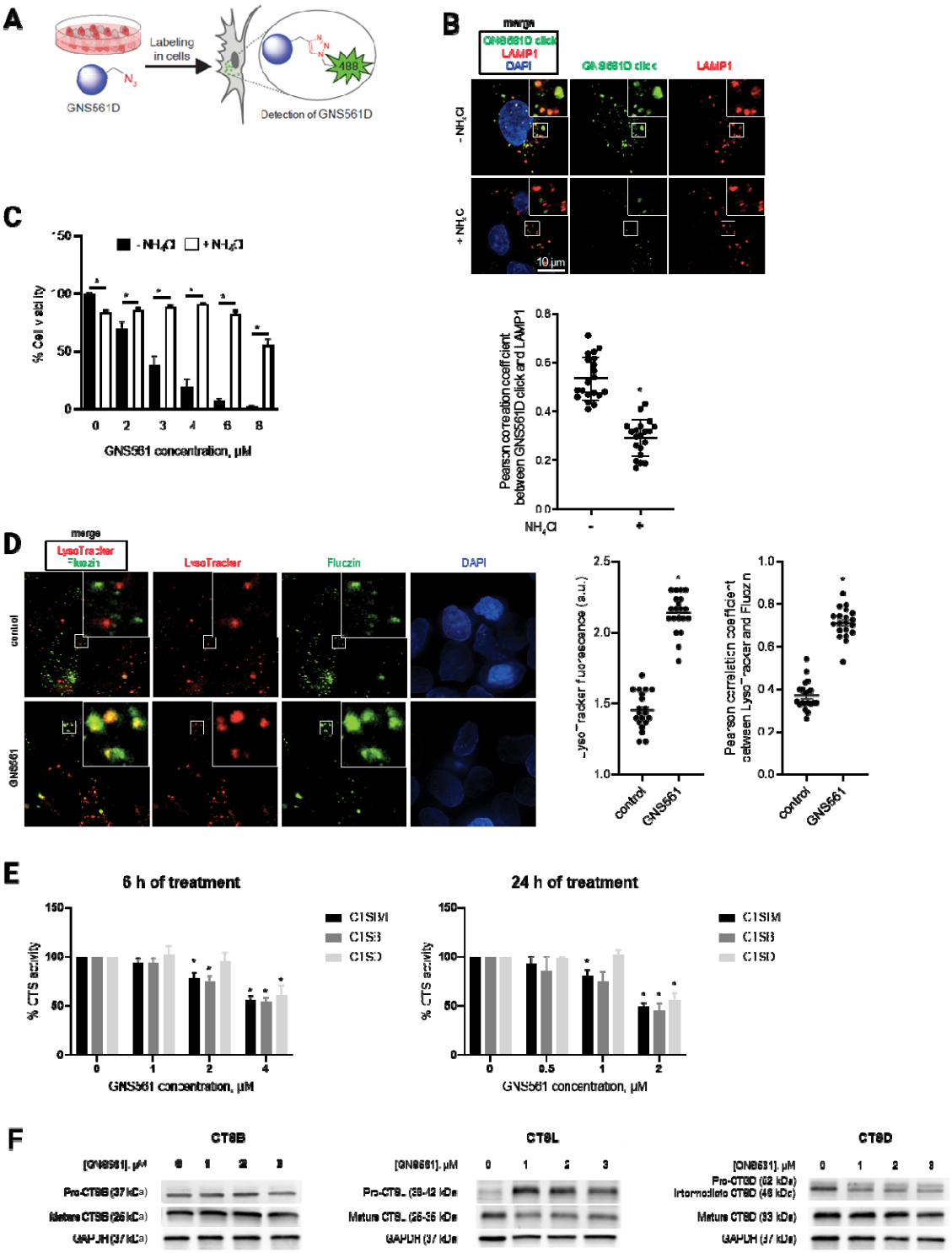

Figure 4. The lysosomotropic agent GNS561 modulates lysosomal functions in the HepG2 cell line. (A) Chemical labeling of GNS561D in cells. (B) Lysosomal localization of GNS561D after NH_4Cl pretreatment (20 mM) for 30 min and then treatment with GNS561D (10 µM) and NH_4Cl (20 mM) for 90 min. (C) Cell viability after 24 h of GNS561 exposure in the

226 presence or absence of NH_4Cl (20 mM). (D) Staining of lysosomes (LysoTracker) and unbound
227 Zn^{2+} (Fluozin) after GNS561 treatment (1 h, 10 µM). Quantification of LysoTracker
228 fluorescence in arbitrary units (a.u.) (middle) and lysosomal unbound Zn^{2+} accumulation by
229 Pearson correlation coefficient between LysoTracker and Fluozin (right). (E) Fold change of
230 peptidase activity of cysteine cathepsins (including both cathepsins B and L) (CTSB/L),
231 cathepsin B (CTSB) and cathepsin D (CTSD) after GNS561 treatment (6 h and 24 h) calculated
232 in comparison with the control condition. (F) Representative immunoblotting of
233 procathepsin B (precursor form) and mature CTSB (left), procathepsin L (precursor form) and
234 mature CTSL (middle) and procathepsin D, intermediate and mature CTSD (right) after
235 GNS561 treatment for 16 h. For all blots, GAPDH was used as a loading control. For all
236 studies, n ≥ 3 biological replicates. Data represent the mean + SEM. For comparison, Student
237 t-test was used for (C), (B) and (D), and one-way ANOVA with Dunnett's post hoc analysis
238 was performed for (E). * represents significant difference, at least $p < 0.05$.
239
240 **GNS561 modulates lysosomal functions**
241 The GNS561 lysosomotropism-dependent cell death prompted us to examine GNS561
242 capacity to modulate lysosomal characteristics and functions.
243 Following continuous exposure to GNS561, staining of LysoTracker, which is a reagent
244 allowing the identification of the lysosomal compartment, increased in HepG2 cells (Figure
245 4D), suggesting that GNS561 prompted a dose-dependent build-up of enlarged lysosomes.
246 We therefore examined the enzymatic activity of three prominent lysosomal proteinases,
247 two cysteine cathepsins B (CTSB) and L (CTSL), and aspartic cathepsin D (CTSD). After 6 and
248 24 h of treatment, GNS561 significantly impaired, in a dose-dependent manner, the
249 enzymatic activity of cathepsins (Figure 4E). However, this decreased activity did not relate
250 to a direct GNS561-dependent inhibition of cathepsin activities (Figure S4). Based on the
251 literature, depressed proteolytic activity of cathepsins may result from an increased Zn^{2+}
252 lysosomal concentration and/or altered maturation of cathepsin precursors. Indeed, it has
253 been described that Zn^{2+} may downregulate the proteolytic activity of CSTB and CTSL
254 (Lockwood 2010, Lockwood 2013, Lockwood 2019). We investigated whether GNS561
255 modified unbound Zn^{2+} localization in HepG2 cells. As shown in Figure 4D, GNS561 induced a
256 strong accumulation of unbound Zn^{2+} in lysosomes, as evidenced by colocalization of the

257 fluorescent signals of Fluozin and LysoTracker in the merged images. This increase in
258 lysosomal unbound Zn^{2+} could explain the decreased proteolytic activity of CTSL and CTSB.
259 Cathepsins are synthesized as inactive zymogens, which are converted to their mature active
260 forms by other proteases or by autocatalytic processing (Turk et al. 2012). As depicted in
261 Figure 4F, GNS561 did not impact CTSB maturation, while it impaired the maturation of both
262 CTSL and CSTD (increase of precursor forms) and decreased their catalytic activity
263 accordingly.

264 As GNS561 induced lysosomal dysfunction, the effect of GNS561 on the autophagic process
265 was investigated. Herein, we showed that the GNS561-induced accumulation of light chain 3
266 phosphatidylethanolamine conjugate was not enhanced in the presence of BafA1 (Figure
267 S5), suggesting that GNS561 blocked autophagic flux.
268

269 **PPT1 is a target of GNS561**

270 Since PPT1 is critical for lysosomal function and is described to be the molecular target of
271 chloroquine derivatives (Rebecca et al. 2017, Rebecca et al. 2019), we investigated whether
272 PPT1 could be a molecular target of GNS561. First, the binding of GNS561 to recombinant
273 PPT1 was analyzed in vitro by nano differential scanning fluorimetry using HCQ as a positive
274 control (Rebecca et al. 2019). In the presence of GNS561 and HCQ, we observed a significant
275 dose-dependent decrease in PPT1 melting temperature (Figure 5A). Additionally, inhibition
276 of PPT1 enzymatic activity was observed in HepG2 cells treated with GNS561 (Figure 5B).
277 Moreover, the chemical mimetic N-*tert*-butylhydroxylamine (NtBuHA) attenuated autophagy
278 inhibition associated with GNS561 (Figure 5C), indicating that inhibition of PPT1 function by
279 GNS561 induced the observed anti-autophagy effect.
280 To determine whether inhibition of PPT1 function was responsible for the antitumoral
281 activity of GNS561, HepG2 cells were treated with GNS561 with or without NtBuHA
282 pretreatment. As shown in Figure 5D, NtBuHA partially prevented the antitumor activity of
283 GNS561, as evidenced by the increased viability of cells pretreated with NtBuHA. The same
284 rescue effect of NtBuHA pretreatment was observed for HCQ used as a positive control
285 (Figure S7). After demonstrating that NtBuHA had no impact on GNS561 lysosomal
286 localization (Figure S6), we validated that the impact of NtBuHA pretreatment was due to its

287 PPT1 mimetism, suggesting that inhibition of PPT1 function by GNS561 was partially liable
288 for its antitumoral activity.
289 The results of Rebecca et al. suggested that PPT1 inhibition could result in mTOR inhibition
290 through the displacement of mTOR from the lysosomal membrane (Rebecca et al. 2017,
291 Rebecca et al. 2019). Thus, we investigated the localization of mTOR after GNS561 treatment
292 using immunofluorescence microscopy. HCQ and EAD1 were used as positive controls (Sironi
293 et al. 2019). As shown in Figure 5E, GNS561 treatment, as well HCQ and EAD1 treatments,
294 significantly impaired mTOR localization to the lysosomal surface. Therefore, GNS561-
295 induced PPT1 inhibition resulted in displacement of mTOR from the lysosomal membrane
296 and consequently likely inhibited the mTOR signaling pathway.

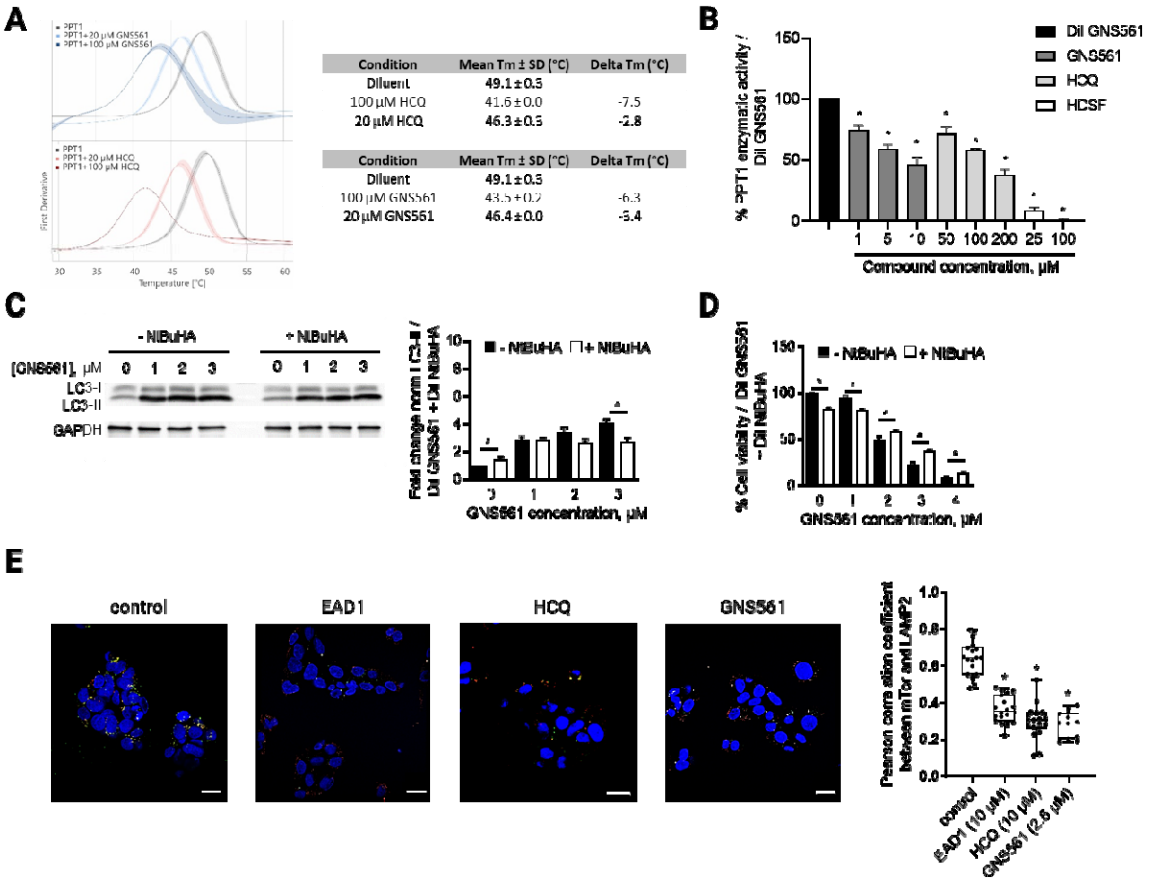

297

298 **Figure 5. GNS561 targets PPT1.** (A) Nano differential scanning fluorimetry assays comparing
299 GNS561 + PPT1 and HCQ + PPT1 against the apo-PPT1 ligand. Data represent the mean (solid
300 lines) ± SEM (shaded areas) of two experiments. (B) PPT1 enzymatic activity of HepG2 cells
301 treated with GNS561 for 3 h. HCQ and HDSF were used as positive controls. The results were
302 compared to the diluent of GNS561 (control condition). (C) Representative immunoblotting

303 of LC3-II in HepG2 cells treated with GNS561 for 16 h in the presence or absence of NtBuHA
304 (8 mM). GAPDH was used as a loading control. Fold changes of normalized LC3-II level were
305 calculated against the control condition (diluent of GNS561 + diluent of NtBuHA). (D) Cell
306 viability percent against the control condition (diluent of GNS561 + diluent of NtBuHA) after
307 24 h of treatment with GNS561 in the presence or absence of NtBuHA (8 mM). (E) Staining of
308 lysosomes (LAMP2, green), mTOR (red) and nucleus (DAPI, blue) after treatment with
309 GNS561 and two positive controls, EAD1 and HCQ, for 16 h. Pearson correlation coefficient
310 between mTOR and LAMP2 was represented using box and whisker representation (min to
311 max). Scale bars represent 20 µm. In (B), (C) and (D), data represent the mean + SEM. For
312 comparison, Student t-test was used for (C) and (D) and one-way ANOVA with Dunnett's
313 post hoc analysis was performed for (B) and (E). For all studies except (A), $n \geq 3$ biological
314 replicates. * represents significant difference, at least $p < 0.05$.
315
316 **GNS561 induces LMP and cathepsin-dependent cell death**
317 To characterize GNS561-induced changes in lysosomes, we analyzed LMP. To this end, we
318 took advantage of the steady endocytic capacity of cells to load fluorescent dextran into
319 lysosomes and the translocation of lysosomal localized dextran into the cytosol after LMP-
320 inducing insult. Fluorescent dextran in healthy cells appears in dense punctate structures
321 representing intact lysosomes, whereas after LMP, a diffuse staining pattern throughout the
322 cytoplasm is seen. After GNS561 treatment, such diffuse dextran staining was observed
323 (Figure 6A), suggesting an induction of LMP. As seen in Figure 6B, the loss of membrane
324 integrity, which is the hallmark of LMP, was observed by transmission electron microscopy of
325 HepG2 cells treated with 3 µM GNS561 for 24 h. To confirm this effect, cathepsin localization
326 was studied after GNS561 treatment. After 48 h of treatment, GNS561 decreased cathepsin
327 staining (Figure 6C), indicating that cathepsins were released into the cytosol, thus validating
328 LMP.
329 As cathepsin release into the cytosol after LMP may trigger cytosolic cellular death signaling
330 (Oberle et al. 2010), we evaluated the role of cathepsins in GNS56-induced cell death. To this
331 end, HepG2 cells were pretreated with an inhibitor of CTSD, pepstatin A, or an inhibitor of
332 CTSB, CA-074-Me. Under these conditions, cell viability was partially rescued (Figure 6D and
333 E), suggesting that the GNS561-induced apoptotic pathway is at least partially cathepsin-
334 dependent.

335

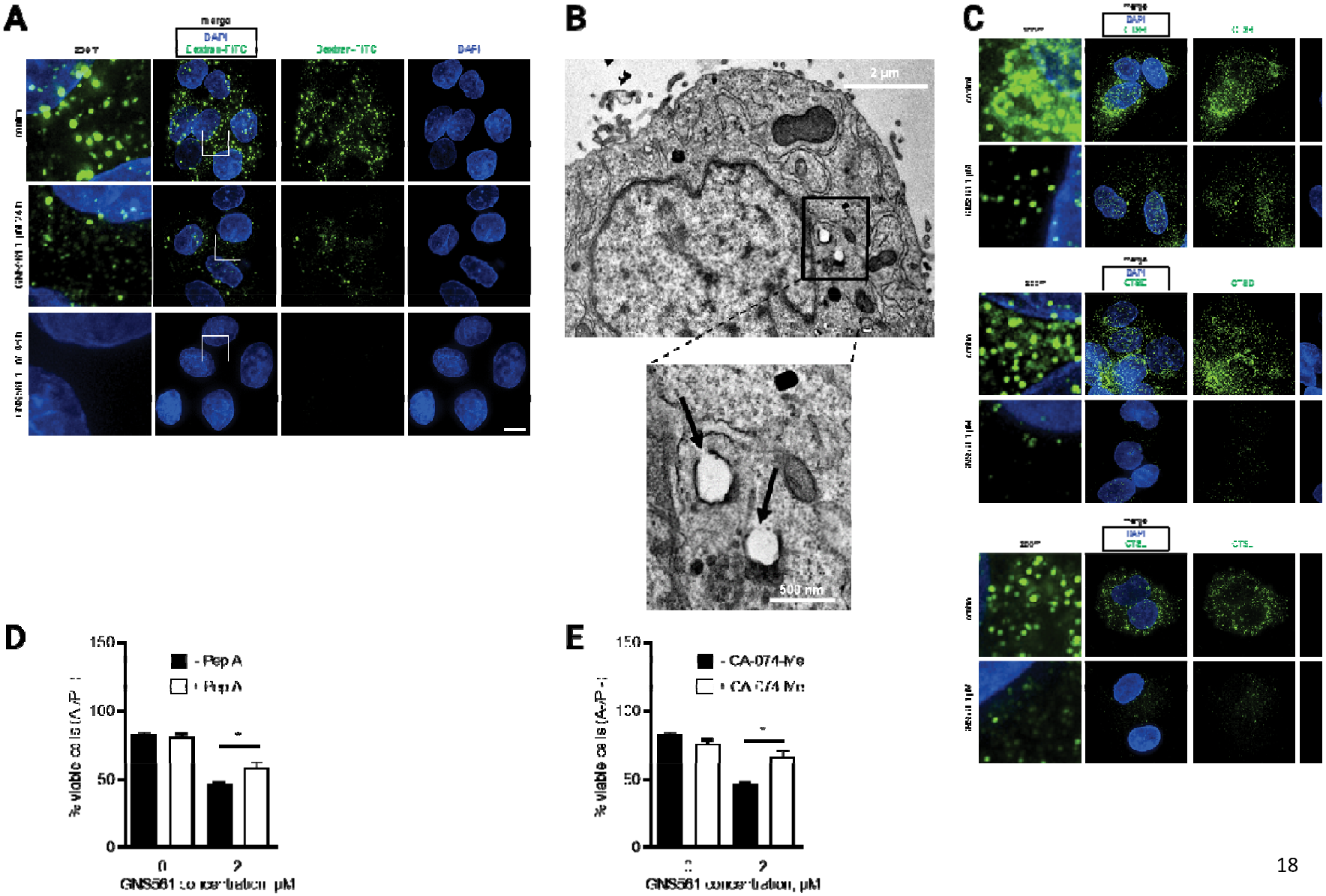
A
merge
DAPI
Dextran-FITC
Dextran-FITC
DAPI
B
2 µm
500 nm
C
merge
DAPI
control
D
150
100
50
0
- Pep A
+ Pep A
0
2
GNS561 concentration, µM
E
150
100
50
0
- CA-074-Me
+ CA-074-Me
2
GNS561 concentration, µM

336

337 **Figure 6. GNS561 induces LMP and cathepsin-dependent cell death in HepG2 cells.** (A)
338 Localization of FITC-dextran after GNS561 treatment for the indicated times. (B) Electron
339 microscopy imaging of lysosomal membrane permeabilization (arrows) after GNS561
340 treatment (3 µM) for 24 h. (C) Localization of cathepsin B (CTSB), cathepsin D (CTSD) and
341 cathepsin L (CTSL) after GNS561 treatment for 48 h. (D) Viable cell (A-/PI-) analysis by flow
342 cytometry of cells pretreated or not with pepstatin A (Pep A) (5 µM) for 1 h and then treated
343 with Pep A (5 µM) and GNS561 or with GNS561 alone for 48 h. (E) Viable cell (A-/PI-) analysis
344 by flow cytometry of cells pretreated or not with CA-074-Me (20 µM) for 1 h and then
345 treated with CA-074-Me (20 µM) and GNS561 or with GNS561 alone for 48 h. Scale bars in
346 (A) and (C) represent 10 µm. For all studies, $n \geq 3$ biological replicates. Data represent the
347 mean + SEM. For comparison, Student t-test was used. * represents significant difference, at
348 least $p < 0.05$.
349
350

351 **DISCUSSION**

352 Rapidly dividing and invasive cancer cells are strongly dependent on effective lysosomal
353 functions. Lysosomes are acidic and catabolic organelles found in nucleated human cells that
354 are responsible for the disposal and recycling of used and damaged macromolecules and
355 organelles, as well as the assimilation of extracellular materials incorporated into the cell by
356 endocytosis, autophagy, and phagocytosis. Increased autophagic flux and changes in
357 lysosomal compartments in cancer cells have been shown to promote invasion, proliferation,
358 tumor growth, angiogenesis, and drug resistance. Consistently, lysosomal changes are
359 expected to sensitize cells to lysosome-targeting anticancer drugs (Kallunki et al. 2013).
360 Many steps in the autophagy pathway represent potentially druggable targets and several
361 clinical trials have aimed to inhibit autophagy by inhibiting lysosomal functions using CQ and
362 HCQ. Unfortunately, CQ and HCQ failed to demonstrate consistent antitumor effects
363 possibly due to subeffective anticancer concentrations in humans, even with high doses.
364 Drug screening led us to identify GNS561 as a lead compound that displays lysosomotropism
365 and significantly higher antiproliferative effects in human cancer cells compared to HCQ.
366 We previously reported that GNS561 yielded antiproliferative activity in iCCA, inhibited late-
367 stage autophagy, and induced a dose-dependent enlargement of lysosomes (Brun et al.
368 2019). Based on these preliminary results, we further investigated the cellular mechanisms
369 by which GNS561 may lead to lysosomal changes and death in cancer cells. In this study, we
370 confirmed that GNS561 antitumor properties are strongly dependent on its lysosomotropic
371 properties. In accordance with the hypothesis proposed in our previous study (Brun et al.
372 2019), we showed here that GNS561 induced a dose-dependent increase in the number of
373 enlarged lysosomes, LMP leading to cytosolic cathepsin release, caspase activation, and
374 apoptotic cell death. These observations confirm prior reports that highlight the capability of
375 lysosomotropic agents to cause lysosomal stress and lysosomal enlargement (Wang et al.
376 2018). Moreover, studies demonstrated that lysosomal unbound Zn^{2+} buildup led to
377 lysosomal swelling, LMP, release of lysosomal enzymes, and cell death (Hwang et al. 2008,
378 Chung et al. 2009, Hwang et al. 2010, Yu et al. 2010). Further investigations are needed to
379 identify the upstream signals that initiate LMP in GNS561-treated cells.
380 PPT1, an enzyme involved in the removal of thioester-linked fatty acyl groups in proteins and
381 thus subsequently enabling the degradation and intracellular trafficking of membrane-bound

382 proteins, plays a central role in the control of cellular autophagy. PPT1 is highly expressed in
383 several cancer cell lines as well as in advanced stage cancers in patients (Rebecca et al.
384 2019). Recent data have shown that lysosome-specific inhibitors targeting PPT1 can
385 modulate protein palmitoylation and display antitumor activity in melanoma and colon
386 cancer models (Rebecca et al. 2017). Our data showed that PPT1 acts as a molecular target
387 of GNS561. GNS561 bound to PPT1 and inhibited its activity in cells. Cells treated with the
388 chemical mimetic NtBuHA were partially resistant to GNS561-mediated cytotoxicity and
389 attenuated GNS561-associated autophagic flux inhibition, suggesting that inhibition of the
390 thioesterase activity of PPT1 is essential for the anti-autophagic and antitumoral effects of
391 GNS561.
392 In our study, we observed that GNS561 modified the intracellular distribution and
393 localization of mTOR. This is in accordance with previous studies showing that inhibition of
394 PPT1 may displace the mTOR protein from the lysosomal membrane as a result of the
395 inhibition of vATPase/Ragulator/Rag GTPase interactions (Sancak et al. 2010, Korolchuk et al.
396 2011, Carroll et al. 2016, Rebecca et al. 2017, Rabanal-Ruiz and Korolchuk 2018, Rebecca et
397 al. 2019, Sironi et al. 2019). It was also described that lysosomal mTORClocalization brings it
398 in close vicinity to its main regulator, Rheb, and that as a result, the mTOR/Rheb interaction
399 can activate mTOR kinase activity leading to the phosphorylation of downstream effectors
400 (Carroll et al. 2016). Consistently, we hypothesized that GNS561-induced PPT1 inhibition led
401 to mTOR signaling pathway inhibition.
402 As previously observed in iCCA (Brun et al. 2019), we showed here that GNS561 induced a
403 significant decrease in the enzymatic activity of cathepsins. This decreased activity is unlikely
404 due to a direct inhibition of CTSL, CTSB and CTSD by GNS561 but rather could be the
405 consequence of both impairment of CTSL and CTSD maturation and lysosomal unbound Zn^{2+}
406 accumulation. As cathepsin activity is optimal in acidic pH (Gieselmann et al. 1985, Turk et al.
407 1999), we could also speculate that GNS561 may negatively influence the proteolytic activity
408 of cathepsins by inducing an increase in lysosomal pH via PPT1 inhibition. In fact, other
409 authors have shown that PPT1 deficiency in Cln1-/- mice disrupted the delivery of the v-
410 ATPase subunit V0a1 to the lysosomal membrane, leading to a dysregulation of lysosomal
411 acidification (Bagh et al. 2016). The authors suggested that S-palmitoylation by PPT1 may
412 play a critical role in the trafficking of the V0a1 subunit of v-ATPase to the lysosomal
413 membrane and in lysosomal pH regulation.

414 Based on prior studies, GNS561 was neither a zinc ionophore nor a zinc chelator (data not
415 shown), unlike CQ (Xue et al. 2014). However, our hypothesis that GNS561-induced PPT1
416 inhibition could lead to lysosomal deacidification could also explain the observed lysosomal
417 unbound Zn^{2+} accumulation after GNS561 treatment. In fact, as lysosomal pH is mainly
418 regulated by cation/anion movement across the lysosomal membrane, it was suggested that
419 a proton motive force was required to mediate unbound Zn^{2+} efflux (Lockwood 2013, Bin et
420 al. 2019).
421 In summary, GNS561-induced PPT1 inhibition may lead to two main mechanisms inducing
422 cancer cell death. One is related to lysosomal deacidification, which induces lysosomal
423 unbound Zn^{2+} accumulation, a decrease in the enzymatic activity of cathepsins, inhibition of
424 autophagic flux, lysosomal swelling, LMP, cathepsin release, and caspase-dependent
425 apoptosis. The other is linked to prevention of the interaction between v-ATPase and the
426 Ragulator complex, blockage of mTOR lysosomal recruitment, impairment of mTOR–Rheb
427 interaction and finally the inhibition of mTOR signaling pathway. Thus, by targeting PPT1,
428 GNS561 acts as a regulator of autophagy and mTOR, two major processes that drive cancer
429 aggressiveness. Finally, as lysosomes and autophagy are associated with adaptive
430 mechanisms of resistance to mTOR inhibition (Xie et al. 2013), GNS561 can disable mTOR
431 function and downregulate adaptive mechanisms of resistance.
432 An extensive preclinical program has been conducted to evaluate the antitumor activity,
433 pharmacological properties and toxicology of GNS561. Our data showed that GNS561
434 displays antiproliferative effects in several human cancer cells (cell lines and primary patient-
435 derived cells) and that GNS561 was more potent than HCQ. Analysis of the whole-body
436 tissue distribution of GNS561 in rats after repeated oral dosing of GNS561 showed that
437 GNS561 was mainly concentrated in the liver, stomach and lung. The data are consistent
438 with the basic lipophilic nature of GNS561 and with studies showing that basic lipophilic
439 drugs show high lysosomal tropism and high uptake in lysosome-profuse tissues, such as the
440 liver and the lung (Daniel and Wójcikowski 1997). As GNS561 had a high liver tropism, the
441 effect of GNS561 on tumor growth in vivo was evaluated using two liver cancer models: one
442 orthotopic human liver cancer xenograft mouse model (with an HCC patient-derived cell line,
443 LI0752) and one DEN-induced cirrhotic rat model with HCC. These studies showed that
444 GNS561 administered by oral gavage was well tolerated up to the doses of 50 mg/kg/day for
445 6 days in mice and up to 15 mg/kg/day for 6 weeks in rats and induced significant antitumor

446 growth activity that was either comparable to or higher than sorafenib. In addition, ina DEN-
447 induced cirrhotic rat model with HCC, the combination of GNS561 with sorafenib exerted an
448 additive effect in controlling tumor progression and cell proliferation. Furthermore, instead
449 of that observed with CQ and HCQ (Harder et al. 2018), the distribution of GNS561 into the
450 central nervous system was limited. Inactivating PPT1 mutations have long been known to
451 induce infantile neuronal cerebral lipofuscinosis and induce retinopathy during childhood
452 (Metelitsina et al. 2016). Germline PPT1 mutations were shown to selectively affect the
453 central nervous system, with no effects in other tissues. Prior clinical experience using CQ
454 and HCQ showed that retinopathy was one of the major toxicities in patients (Marmor et al.
455 2011). Authors have suggested that novel PPT1 inhibitors may take advantage of not
456 crossing the blood-brain barrier to avoid retinal toxicity (Rebecca et al. 2019). Interestingly,
457 our data shown that the disposition of GNS561 displays limited penetration into the brain in
458 rats, consistent with the lack of neurological and retinal toxicity observed in the current
459 Phase 1b/2a clinical trial of GNS561 (ClinicalTrials.gov).
460 In brief, our findings strengthen the importance of PPT1 and lysosomes as cancer targets.
461 Recently, it was shown that PPT1 inhibition by CQ derivatives or genetic Ppt1 inhibition
462 increases the antitumor activity of anti-PD-1 antibody in melanoma by M2 to M1 phenotype
463 switching in macrophages and a reduction in myeloid-derived suppressor cells in the tumor
464 (Sharma et al. 2020). As such, GNS561 represents a promising new candidate for drug
465 development in HCC either alone or in combination with other drugs, such as anti-PD-1
466 antibody.
467

468 **METHODS**

469 Details of the materials and methods are provided in the Supplementary Methods.

470

471 *Cell culture*

472 All cell lines were cultured in the presence of 5% CO_2 and 95% air in a humidified incubator
473 and were maintained in medium containing 1% penicillin-streptomycin (Dutscher, #P06-
474 07100) and 10% fetal bovine serum (HyClone, #SV30160.03C), except NIH:OVCAR3 and KG-1
475 cell lines, which were cultured in medium supplemented with 20% fetal bovine serum.

476

477 *Animal models*

478 The animals were checked daily for clinical signs, effects of tumor growth and any other
479 abnormal effects. For experiments involving the mouse model (performed in CrownBio
480 facilities), the protocol and any amendment(s) or procedures involving the care and use of
481 animals were reviewed and approved by the Institutional Animal Care and Use Committee of
482 CrownBio prior to experimentation, and during the study, the care and use of animals was
483 conducted in accordance with the regulations of the Association for Assessment and
484 Accreditation of Laboratory Animal Care. For the rat model, all animals received humane
485 care in accordance with the Guidelines on the Humane Treatment of Laboratory Animals
486 (Directive 2010/63/EU), and experiments were approved by the animal Ethics Committee:
487 GIN Ethics Committee No.004.

488

489 *Statistical analysis*

490 Statistical analyses were performed using Prism 8.4.3 software (GraphPad Software Inc., CA,
491 USA). For datasets with normal distribution, multiple comparisons were performed using
492 one-way ANOVA with Dunnett's post hoc analysis. The parametric Student t-test was used to
493 compare two groups of data with normal distribution. Data are presented as the mean
494 values ± standard error mean (SEM) unless stated otherwise. Statistical significance was
495 defined as a p-value < 0.05 and has been indicated by an asterisk in all figures.

496

497

SUPPLEMENTAL INFORMATION

Supplemental Information can be found online.

ACKNOWLEDGMENTS

The authors are very grateful to Dr. Sebastian Müller and Dr. Raphaël Rodriguez from Curie Institute for mechanistic analysis, Pr. Thierry Levade and Dr. Nathalie Andrieu from CRCT for the PPT1 enzymatic assay, Keerthi Kurma and Seyedeh Tayebeh Ahmad Pour for the Institute for Advanced Biosciences for technical support during animal experiments and Dr. François Autelitano, Dr. Marie Guillemot and Philippe Fabre for Zn^{2+} localization analysis.

AUTHOR CONTRIBUTIONS

Conceptualization, S.B, E.R, F.B and P.H.; Methodology, S.B., F.B., T.D, P.H; Validation, S.B., Z.M.J, G.L, J.S, T.S, T.D; Formal Analysis, S.B., Z.M.J, M.N, J.T, A.H, G.L, R.L, T.S, M.G.P, J.P.B; Investigation, Z.M.J, S.M., M.N, J.T, A.H, L.V, E.B, R.L, M.G.P, G.R; Resources, J.C, C.A; Data Curation, C.D, G.J; Visualization, S.B, Z.M.J; Supervision, S.B, F.B, P.H; Project Administration, S.B; Writing – original draft preparation, S.B.; Writing – review and editing, S.B., E.R, F.B., Z.M.J, M.R, G.L, C.S, and P.H.; Funding Acquisition, P.H.

DECLARATION OF INTERESTS

SB, ER, FB, SM, MR, MN, JT, EB, JC, CD, GJ, CS, CA and PH are employees of Genoscience Pharma. SB, ER, FB, CD, CS, CA and PH are shareholders of Genoscience Pharma. SB, FB, JC and PH are co-inventors of a pending patent. The other authors declare no competing interests.

522 **REFERENCES**

523 Aits, S. and Jaattela, M. (2013). Lysosomal cell death at a glance. Journal of Cell Science
524 126(9): 1905-1912.
525
526 Bagh, M.B., Peng, S., Chandra, G., Zhang, Z. and Mukherjee, A.B. (2016). Dysregulation of V-
527 ATPase Function Impairs Lysosomal Acidification in a Mouse Model of a Rare Lysosomal
528 Storage Disease, INCL. The FASEB Journal 30(1_supplement): 879.871-879.871.
529
530 Bin, B.-H., Lee, S.-H., Bhin, J., Irié, T., Kim, S., Seo, J., Mishima, K., Lee, T.R., Hwang, D.,
531 Fukada, T., et al. (2019). The epithelial zinc transporter ZIP10 epigenetically regulates human
532 epidermal homeostasis by modulating histone acetyltransferase activity. The British Journal
533 of Dermatology 180(4): 869-880.
534
535 Bray, F., Ferlay, J., Soerjomataram, I., Siegel, R.L., Torre, L.A. and Jemal, A. (2018). Global
536 cancer statistics 2018: GLOBOCAN estimates of incidence and mortality worldwide for 36
537 cancers in 185 countries. CA: a cancer journal for clinicians 68(6): 394-424.
538
539 Brun, S., Bassissi, F., Serdjebi, C., Novello, M., Tracz, J., Autelitano, F., Guillemot, M., Fabre,
540 P., Courcambeck, J., Ansaldi, C., et al. (2019). GNS561, a new lysosomotropic small molecule,
541 for the treatment of intrahepatic cholangiocarcinoma. Investigational New Drugs 37(6):
542 1135-1145.
543
544 Carroll, B., Maetzel, D., Maddocks, O.D., Otten, G., Ratcliff, M., Smith, G.R., Dunlop, E.A.,
545 Passos, J.F., Davies, O.R., Jaenisch, R., et al. (2016). Control of TSC2-Rheb signaling axis by
546 arginine regulates mTORC1 activity. eLife 5.
547
548 Chung, H., Yoon, Y.H., Hwang, J.J., Cho, K.S., Koh, J.Y. and Kim, J.-G. (2009). Ethambutol-
549 induced toxicity is mediated by zinc and lysosomal membrane permeabilization in cultured
550 retinal cells. Toxicology and Applied Pharmacology 235(2): 163-170.
551
552 ClinicalTrials.gov. " Study of GNS561 in Patients With Liver Cancer." ClinicalTrials.gov.
553
554 Daniel, W.A. and Wójcikowski, J. (1997). Contribution of lysosomal trapping to the total
555 tissue uptake of psychotropic drugs. Pharmacology & Toxicology 80(2): 62-68.
556
557 Dolgin, E. (2019). Anticancer autophagy inhibitors attract 'resurgent' interest. Nature
558 Reviews. Drug Discovery 18(6): 408-410.
559
560 Gieselmann, V., Hasilik, A. and von Figura, K. (1985). Processing of human cathepsin D in
561 lysosomes in vitro. The Journal of Biological Chemistry 260(5): 3215-3220.
562
563 Harder, B.G., Blomquist, M.R., Wang, J., Kim, A.J., Woodworth, G.F., Winkles, J.A., Loftus, J.C.
564 and Tran, N.L. (2018). Developments in Blood-Brain Barrier Penetrance and Drug
565 Repurposing for Improved Treatment of Glioblastoma. Frontiers in Oncology 8.
566
567 Hwang, J.J., Kim, H.N., Kim, J., Cho, D.-H., Kim, M.J., Kim, Y.-S., Kim, Y., Park, S.-J. and Koh, J.-
568 Y. (2010). Zinc(II) ion mediates tamoxifen-induced autophagy and cell death in MCF-7 breast

569 cancer cell line. Biometals: An International Journal on the Role of Metal Ions in Biology,
570 Biochemistry, and Medicine 23(6): 997-1013.
571
572 Hwang, J.J., Lee, S.-J., Kim, T.-Y., Cho, J.-H. and Koh, J.-Y. (2008). Zinc and 4-hydroxy-2-
573 nonenal mediate lysosomal membrane permeabilization induced by H2O2 in cultured
574 hippocampal neurons. The Journal of Neuroscience: The Official Journal of the Society for
575 Neuroscience 28(12): 3114-3122.
576
577 Kallunki, T., Olsen, O.D. and Jäättelä, M. (2013). Cancer-associated lysosomal changes:
578 friends or foes? Oncogene 32(16): 1995-2004.
579
580 Kimura, T., Takabatake, Y., Takahashi, A. and Isaka, Y. (2013). Chloroquine in cancer therapy:
581 a double-edged sword of autophagy. Cancer Research 73(1): 3-7.
582
583 Klempner, S.J., Myers, A.P. and Cantley, L.C. (2013). What a tangled web we weave:
584 emerging resistance mechanisms to inhibition of the phosphoinositide 3-kinase pathway.
585 Cancer Discovery 3(12): 1345-1354.
586
587 Korolchuk, V.I., Saiki, S., Lichtenberg, M., Siddiqi, F.H., Roberts, E.A., Imarisio, S., Jahreiss, L.,
588 Sarkar, S., Futter, M., Menzies, F.M., et al. (2011). Lysosomal positioning coordinates cellular
589 nutrient responses. Nature Cell Biology 13(4): 453-460.
590
591 Lockwood, T.D. (2010). The lysosome among targets of metformin: new anti-inflammatory
592 uses for an old drug? Expert Opinion on Therapeutic Targets 14(5): 467-478.
593
594 Lockwood, T.D. (2013). Lysosomal metal, redox and proton cycles influencing the CysHis
595 cathepsin reaction. Metallomics: Integrated Biometal Science 5(2): 110-124.
596
597 Lockwood, T.D. (2019). Biguanide is a modifiable pharmacophore for recruitment of
598 endogenous Zn2+ to inhibit cysteinyl cathepsins: review and implications. Biometals: An
599 International Journal on the Role of Metal Ions in Biology, Biochemistry, and Medicine 32(4):
600 575-593.
601
602 Manic, G., Obrist, F., Kroemer, G., Vitale, I. and Galluzzi, L. (2014). Chloroquine and
603 hydroxychloroquine for cancer therapy. Molecular & Cellular Oncology 1(1): e29911.
604
605 Marmor, M.F., Kellner, U., Lai, T.Y.Y., Lyons, J.S., Mieler, W.F. and Ophthalmology, A.A.o.
606 (2011). Revised recommendations on screening for chloroquine and hydroxychloroquine
607 retinopathy. Ophthalmology 118(2): 415-422.
608
609 Metelitsina, T.I., Waggoner, D.J. and Grassi, M.A. (2016). BATTEN DISEASE CAUSED BY A
610 NOVEL MUTATION IN THE PPT1 GENE:. Retinal Cases & Brief Reports 10(3): 211-213.
611
612 Oberle, C., Huai, J., Reinheckel, T., Tacke, M., Rassner, M., Ekert, P.G., Buellesbach, J. and
613 Borner, C. (2010). Lysosomal membrane permeabilization and cathepsin release is a
614 Bax/Bak-dependent, amplifying event of apoptosis in fibroblasts and monocytes. Cell Death
615 and Differentiation 17(7): 1167-1178.

616
617 Pascolo, S. (2016). Time to use a dose of Chloroquine as an adjuvant to anti-cancer
618 chemotherapies. European Journal of Pharmacology 771: 139-144.
619
620 Pérez-Hernández, M., Arias, A., Martínez-García, D., Pérez-Tomás, R., Quesada, R. and Soto-
621 Cerrato, V. (2019). Targeting Autophagy for Cancer Treatment and Tumor
622 Chemosensitization. Cancers 11(10): 1599.
623
624 Plantone, D. and Koudriavtseva, T. (2018). Current and Future Use of Chloroquine and
625 Hydroxychloroquine in Infectious, Immune, Neoplastic, and Neurological Diseases: A Mini-
626 Review. Clinical Drug Investigation 38(8): 653-671.
627
628 Rabanal-Ruiz, Y. and Korolchuk, V.I. (2018). mTORC1 and Nutrient Homeostasis: The Central
629 Role of the Lysosome. International Journal of Molecular Sciences 19(3).
630
631 Rebecca, V.W., Nicastri, M.C., Fennelly, C., Chude, C.I., Barber-Rotenberg, J.S., Ronghe, A.,
632 McAfee, Q., McLaughlin, N.P., Zhang, G., Goldman, A.R., et al. (2019). PPT1 Promotes Tumor
633 Growth and Is the Molecular Target of Chloroquine Derivatives in Cancer. Cancer Discovery
634 9(2): 220-229.
635
636 Rebecca, V.W., Nicastri, M.C., McLaughlin, N., Fennelly, C., McAfee, Q., Ronghe, A., Nofal,
637 M., Lim, C.-Y., Witze, E., Chude, C.I., et al. (2017). A Unified Approach to Targeting the
638 Lysosome's Degradative and Growth Signaling Roles. Cancer Discovery 7(11): 1266-1283.
639
640 Sancak, Y., Bar-Peled, L., Zoncu, R., Markhard, A.L., Nada, S. and Sabatini, D.M. (2010).
641 Ragulator-Rag complex targets mTORC1 to the lysosomal surface and is necessary for its
642 activation by amino acids. Cell 141(2): 290-303.
643
644 Sharma, G., Ojha, R., Noguera-Ortega, E., Rebecca, V.W., Attanasio, J., Liu, S., Piao, S., Lee,
645 J.J., Nicastri, M.C., Harper, S.L., et al. (2020). PPT1 inhibition enhances the antitumor activity
646 of anti-PD-1 antibody in melanoma. JCI insight 5(17).
647
648 Shi, T.-T., Yu, X.-X., Yan, L.-J. and Xiao, H.-T. (2017). Research progress of hydroxychloroquine
649 and autophagy inhibitors on cancer. Cancer Chemotherapy and Pharmacology 79(2): 287-
650 294.
651
652 Sironi, J., Aranda, E., Nordstrøm, L.U. and Schwartz, E.L. (2019). Lysosome Membrane
653 Permeabilization and Disruption of the Molecular Target of Rapamycin (mTOR)-Lysosome
654 Interaction Are Associated with the Inhibition of Lung Cancer Cell Proliferation by a
655 Chloroquinoline Analog. Molecular Pharmacology 95(1): 127-138.
656
657 Turk, B., Dolenc, I., Lenarcic, B., Krizaj, I., Turk, V., Bieth, J.G. and Björk, I. (1999). Acidic pH as
658 a physiological regulator of human cathepsin L activity. European Journal of Biochemistry
659 259(3): 926-932.
660

661 Turk, V., Stoka, V., Vasiljeva, O., Renko, M., Sun, T., Turk, B. and Turk, D. (2012). Cysteine
662 cathepsins: From structure, function and regulation to new frontiers. Biochimica et
663 Biophysica Acta (BBA) - Proteins and Proteomics 1824(1): 68-88.
664
665 Verbaanderd, C., Maes, H., Schaaf, M.B., Sukhatme, V.P., Pantziarka, P., Sukhatme, V.,
666 Agostinis, P. and Bouche, G. (2017). Repurposing Drugs in Oncology (ReDO)-chloroquine and
667 hydroxychloroquine as anti-cancer agents. Ecancermedicalscience 11: 781.
668
669 Wang, F., Gómez-Sintes, R. and Boya, P. (2018). Lysosomal membrane permeabilization and
670 cell death. Traffic 19(12): 918-931.
671
672 Xie, X., White, E.P. and Mehnert, J.M. (2013). Coordinate Autophagy and mTOR Pathway
673 Inhibition Enhances Cell Death in Melanoma. PLOS ONE 8(1): e55096.
674
675 Xu, R., Ji, Z., Xu, C. and Zhu, J. (2018). The clinical value of using chloroquine or
676 hydroxychloroquine as autophagy inhibitors in the treatment of cancers: A systematic review
677 and meta-analysis. Medicine 97(46): e12912.
678
679 Xue, J., Moyer, A., Peng, B., Wu, J., Hannafon, B.N. and Ding, W.-Q. (2014). Chloroquine Is a
680 Zinc Ionophore. PLoS ONE 9(10): e109180.
681
682 Yu, L., McPhee, C.K., Zheng, L., Mardones, G.A., Rong, Y., Peng, J., Mi, N., Zhao, Y., Liu, Z.,
683 Wan, F., et al. (2010). Termination of autophagy and reformation of lysosomes regulated by
684 mTOR. Nature 465(7300): 942-946.
685
686 Zhang, Y., Liao, Z., Zhang, L.-j. and Xiao, H.-t. (2015). The utility of chloroquine in cancer
687 therapy. Current Medical Research and Opinion 31(5): 1009-1013.

688